EXPERIMENTAL EFFECTS OF COAL-LIMESTONE MIXTURES ON DUST DISPERSION BEHIND A MOVING SHOCK WAVE

A Thesis

by

HOWARD GREGORY JOHNSTON

Submitted to the Office of Graduate and Professional Studies of
Texas A&M University
in partial fulfillment of the requirements for the degree of

MASTER OF SCIENCE

Chair of Committee,	Eric L. Petersen
Co-chair of Committee,	M. Sam Mannan
Committee Members,	Young-Joe Kim
Head of Department,	Andreas Polycarpou

December 2015

Major Subject: Mechanical Engineering

ABSTRACT

Secondary dust explosions in coal mines or industrial settings are known to cause greater catastrophic hazards than the coupled primary explosions themselves. The shock waves produced during a primary explosion, which are initiated by inadvertent stimuli in an explosive atmosphere such as methane, lift surrounding coal particles from neighboring areas, and if added in an effort to create an inert mixture, limestone as well. Dust dispersion can influence the severity of a secondary explosion as the particles can ignite from passing shock waves. A shock tube modified to evaluate dust dispersion provides the optical access to characterize the shock-wave/dust-layer interaction. This experimental study characterized the dust dispersion of coal-limestone mixtures and moisture-varied limestone dust as it is likely present in the hazardous environment. The dust rise height was measured with respect to time after the shock passage, where regardless of the sample, initial laminar dust growth rates increased with Mach number. Laminar and unstable regimes were also identified in the data samples.

The moisture-varied limestone samples were tested at three shock Mach numbers, namely M_s = 1.1, 1.23, and 1.4, and the trending data show an average increase of 10% in overall lifting heights and 20% in initial linear growth rates for the moisture-reduced, dried samples as compared to undried samples stored in standard temperature and pressure (STP) conditions. Conceivably, the effective moisture reduction in the samples led to fewer agglomerations and/or reduced densities, influencing the ability of

lift forces to act on the particles. In addition, limestone may bond or agglomerate more readily to coal particles when undried, reducing the likelihood of ignition.

The coal-limestone mixture samples were tested at two shock Mach numbers, namely M_s = 1.24 and 1.57, with the 75% coal sample having the largest and 25% coal sample having the smallest combined dust dispersion parameters. Dust dispersion parameters affect how quickly the dust transitions to an unstable interface layer, readily increasing the chances of ignition through increased mixing and dispersion. As the limestone content is increased, dust grows faster, larger, and tend to transition into larger instabilities on the dust-gas boundaries. The highest dust growth rate, shortest transition time, and largest average dust height will affect the ability of the dust sample to ignite. Increasing undried limestone content while maintaining the lowest possible dust dispersion would both help the mixture remain inert and expose less coal particle surface area to the reactive atmosphere. These parameters are fluid-particle dispersion dynamics.

DEDICATION

I dedicate my work and life to the world and universe that know no boundaries, and can imagine and embrace the hope that we all share for a great life and existence. Always know…who you are.

ACKNOWLEDGMENTS

I would like to thank my mother for her encouragement and her ability to help me follow my dreams. She has been a shining light in my life, and will always be. I thank my sister for supporting me, and always giving me a good laugh to keep good humor in life. Our family grew up in Orlando FL, and included many good times with friends and family over the years.

I would specially like to thank Dr. Eric Petersen for our 10 years of friendship. I noticed when I first met him, as he taught me undergraduate aerospace engineering classes that he was special, and that hasn't changed. He brought me in as a student in his research facility last year, and I haven't regretted one moment since then. I had the pleasure of working with him on a few projects, and was able to take his combustion class my last semester at Texas A&M.

Also, a big thank you to my committee members for supporting me through this research. I know they do everything they can to keep our research and learning facilities running, and I truly thank you for this. I could not do what I love to do without their commitment to Texas A&M. A special thanks to Andrew Demko for spending his time and energy acquiring the SEM images presented herein.

Lastly, and certainly not least, to my loving and kind girlfriend Christina Mittnacht, I am so glad to be traveling life's roads with you. Thank you for all your encouragement and great ideas! I'm sure glad we met, and I can't wait for our future. I love you, always and forever.

TABLE OF CONTENTS

Page

LIST OF FIGURES

Page

LIST OF TABLES

Page

1. INTRODUCTION

An explosive atmosphere can exist in coal mines or other industrial settings where gases like methane are released into the atmosphere as a by-product of coal extraction and processing. In these environments, coal particles are found on floors and other surfaces. The potential of mining equipment, and other apparatus, to inadvertently ignite gases such as methane, can lead to detonations or explosive events that initiate shock waves in the environment called primary explosions.

1.1 Background

Shock waves created during the primary explosion can traverse the near area and pick up coal dust particles left from processing activities, creating a secondary explosion hazard. In the event that these events occur in series, the resulting fuel-air mixture behind the shock wave brings about a potential to ignite the coal particles if a secondary ignition source is present. As this situation has occurred in the past, it is a well-known fact that safety mitigation is necessary to protect life and business operations from this occurrence. Dust explosion hazards are therefore explored in the material presented herein, and represent the experimental effects of dust dispersion due to differing shock wave speeds. In particular, a safety mitigation strategy of spreading limestone in these areas where the coal dust is located is chosen to render the dust mixture inert, and

prevent it from igniting in the event of a shock wave traversing the area. The procedure that creates the shock wave can follow the sequence below:

1. Methane gas is released as by-product of mining or industrial processing
2. Equipment produces friction\spark, igniting methane primary explosion
3. Detonation or deflagrating wave produced from primary explosion
4. Pressure wave continues beyond boundary of reactive gas
5. Shock wave propagates in air, along adjacent surfaces
6. Shock wave disperses dust and increases air temperature with one (1) possibility of two (2) of the following outcomes:
    a. A coal-limestone mixture exhibits partial or no reaction
    b. A coal only dust ignites and creates a secondary explosion

The primary explosion, a result of the methane gas ignition, is the source for the secondary explosion. Once the secondary explosion has momentum, it can lead to a disastrous event such as a detonation wave, killing people and damaging much of the surrounding area. The mitigation strategy involves spreading the limestone to these areas to mitigate any such occurrence. Methane gas explosions in a coal mine are only one possible initiation source, and others should be considered as well.

1.2 Experimental Study Review

As stated, the dispersion of coal dust by a shock wave can create a secondary explosion. The current experimental study targets dust dispersion, and seeks to cover a

range of coal-limestone mixtures that might occur in the field. This information can give safety and simulation experts data to better predict dust dispersions, after explosive conditions are determined from knowledge of the environments considered. This dust explosion hazard study will focus on correlating data for those who are interested in dust dispersion parameters with known shock wave Mach numbers, which can be used to calibrate models that predict the ignition of coal dust in that environment.

In his review paper, Eckhoff [1] discussed prevention and mitigation efforts for secondary explosion hazards along with the importance of modeling dust dispersion in predicted environments. Knowledge of critical dust coverage which would lead to catastrophic explosions is needed to set safety standards. Current methods to mitigate explosive atmospheres include spreading limestone in these areas to create an inert mixture if such an accident were to occur, therefore limiting the possibility of a secondary explosion. Being able to predict or model numerically the dust dispersion behind a passing normal shock wave is therefore important, and high-quality experimental data are needed to validate such models. Dust-layer surface depth, coal-limestone mixtures, and moisture content do have important effects on the lifting height, as their affects are illustrated herein.

To predict dust entrainment into the post-shock gas flow, it is important to understand the initial motion of the particles. Previous work has been performed to enrich the fundamental knowledge of dust dispersion. However, it is still difficult to completely describe the dust entrainment mechanism. A conclusive model to accurately simulate the exact entrainment process has yet to be developed, although some recent

numerical models that capture the details of the shock-dust interaction are appearing in the literature [2,3]. Therefore, to ensure safety regarding dust explosion hazards, it is important to study the dust-lifting process experimentally and identify important parameters that will be valuable for development and validation of numerical predictions of this phenomenon. Former experimental works have studied the interaction of unsteady dust layers with different elements of gas-dynamic flows (e.g., shock, compression and expansion waves).

Earlier shock and dust particle interaction experiments focused on understanding the phenomenon of dust lifting [3]-[11]. For example, Fletcher's [5] explanation of the mechanism of dust lifting was based on experiments as well as theoretical analysis. He criticized Gerrard's [4] conclusion that dust entrainment is under the action of a shock wave passing through the dust layer. Instead, he concluded that the dust is lifted by the rapid flow behind the propagating shock. Bracht and Merzkirch [6] identified the governing force in dust lifting as the Saffman force and supported their experimental work with a numerical model. The behavior of a coal-dust layer with a weak shock wave passing above it was studied by Hwang [7]; the coal dust particle size was up to 44 μm in that work. Later, the effect of particle size on dust dispersion [8] and Magnus force [9] were studied. Fedorov [10] in his review paper discussed the available body of work related to shock interaction with dust layers. According to Federov's conclusion, the dust lifting from a packed bed does not depend on the layer depth. However, curving of the layer surface and particle density do have important effects on the lifting height.

Some of the other studies focused on the dust-lifting problem in conjunction with combustion problems and with detonation, which is usually called a layered detonation. In 2005 and 2012, Klemens et al. studied shock interaction with coal dust and silica dust in a shock tube to identify important parameters such as the time delay in lifting the dust from the layer and the dust concentration gradient behind the propagating shock [11]. For the numerical part of their research, they considered two approaches: Eulerian and Lagrangian for modeling the dispersion of coal dust.

In spite of all the efforts, it is still difficult to describe the dust entrainment mechanism, and moreover, detailed data are still needed. As a result, a comprehensive model to simulate the exact entrainment process is yet to be demonstrated. The processes of dust lifting and two-phase flows were also comprehensively studied numerically [1,2,10-19]. Nonetheless, there is no mathematical model that can describe all stages of the process of dust lifting, including the propagation of waves on the layer, the processes of turbulent mixing, and the specific features of the force interaction of the phases [10]. However, using an Eulerian framework for computation, the very recent Houim and Oran [2] results trended well with recent data from the facility described herein at M = 1.4 that were presented at a conference in 2014. Such a result shows promise in the ability to eventually model the phenomenon and the need for data such that the facility described in the present paper can provide. In addition, advancements in high-speed imaging have made possible the accumulation of large amounts of time-dependent dust growth data.

With these issues is mind, the current experimental study takes different mixtures of coal and limestone and varies the content by weight to see the effects on shock Mach numbers of M_s = 1.24 and 1.57. Also, limestone dust moisture content reduction is experimented to understand its effects at M_s = 1.1, 1.24, and 1.4. These particular M_s values were targeted for their range in possible shock speeds experienced in the actual environment. The parameters measured herein were shock Mach number (M_s), time (ms), dust height (Y_d in mm), coal-limestone mixture weight percentages, Limestone moisture content, particle sizes (μm), dust growth rates ($\frac{dY_d}{dt}$), and correlation parameters linking M_s and dust growth rates together.

The experimental facilities included a shock tube, which propagates a shock wave over a dust layer. The dust dispersion was then measured by optical equipment, which was processed to construct time-varied results. The experimental techniques sought to consolidate possible dust dispersions encountered in industrial settings, as they can then be modeled by simulation, to better predict the physics of the phenomena.

This thesis is constructed to evaluate the parameters as discussed and includes relevant test hardware, data analysis, and results. The thesis is divided as follows. First, the test facility hardware, measurement techniques, and the dust dispersion setup are discussed. Next, material characterization of the limestone only and coal-limestone mixtures are evaluated by SEM images showing particle sizes and dust interaction. Finally, the experimental data show dust growth behavior, and this is followed with the conclusion of results.

2. EXPERIMENTAL SETUP

This section consists of the details of the shock-tube hardware and the procedures for performing the shock-wave/dust-layer interaction experiments. Described first is the shock-tube facility. Next, details on the technique for quantitative measurement of the dust height as a function of time are discussed using high-speed imaging and custom photo processing. Finally, the dust-layer setup inside the shock tube is presented. Detailed assessment of the shock tube is discussed in Chowdhury et al. [20].

2.1 Shock-Tube Facility

The shock tube utilized for this study is ideal because its driven section is square in cross section. The key features of the test section include a large-windowed region for viewing the experiment. This test section is designed to handle incident-shock velocities up to $M_s = 2$ with an initial pressure of 1 atm (101.3 kPa), and it is capable of holding pressures up to 15 atm (1.52 MPa) behind the reflected shock wave. A schematic of the shock tube is provided in Fig. 1.

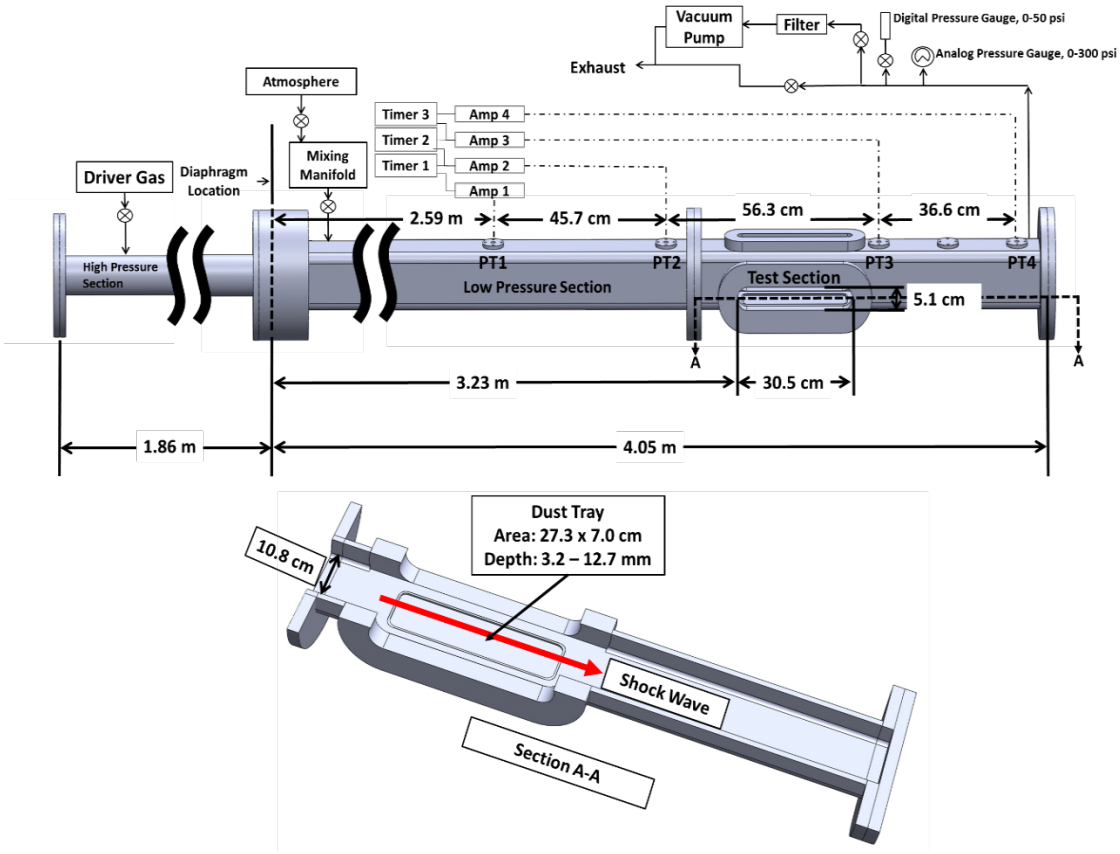

Figure 1 Shock-tube schematic (top) showing plumbing, relative distances, test-port location, 4 pressure transducers (PT1 – PT4), 3 velocity-detection timers, and a section-cut of the dust-layer test section (bottom).

Figure 1 (in the section view) shows the test section located at the end of the shock tube where the dust is leveled coincident with the incident shock wave path. Care is taken to create a uniform layer while minimizing compaction. At nominal test shock speeds, experiments up to 3 ms are achieved. The driven section, where the dust-layer test section is located, is approximately 10.8×10.8 cm and 4.05 meters long. The left and right windows are each 5.1×30.5 cm and allow for viewing of the dust layer and fluid interface, particularly for shadowgraph techniques. Dust is placed in an easy-to-remove

dust pan with a dust deposit area of 27.3×7.0 cm. Figure 2 shows a photograph of the shock-tube facility test section.

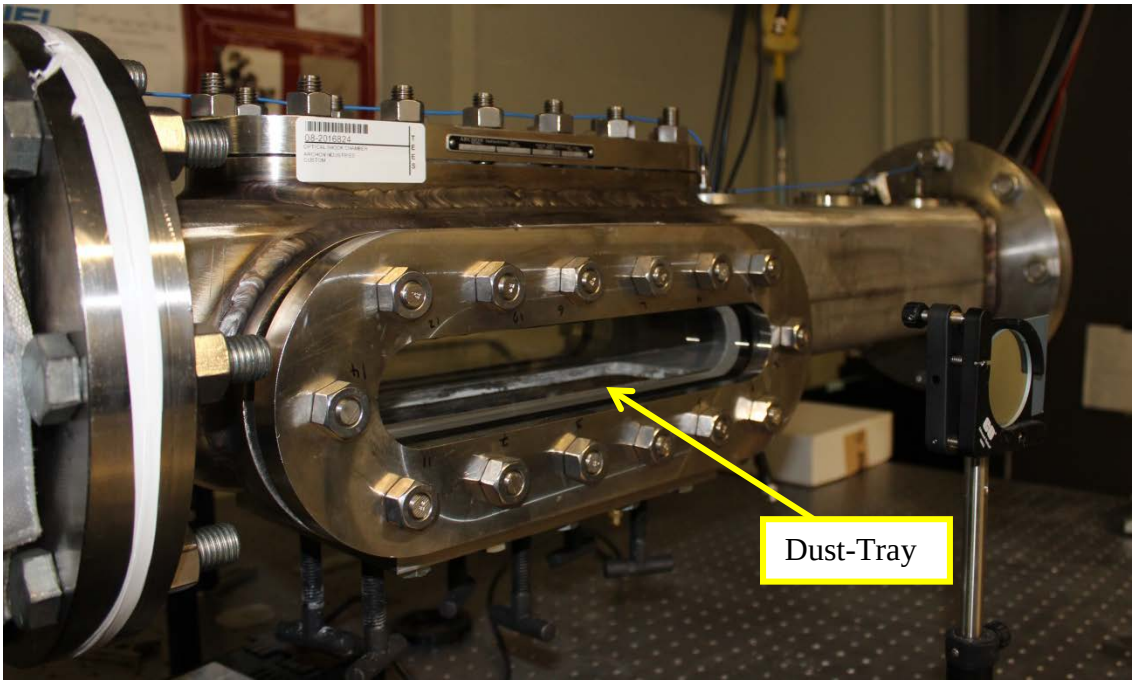

Figure 2 Photograph of shock-tube test section

The shock velocity is determined by a series of pressure transducers connected to three timing gates (Fluke PM6666 counters), depicted schematically in Fig. 1. Of the three timing intervals, one is before the dust-layer test section, one spans the test section, and one is after the test section. The shock wave velocity in the facility characterization discussed in Chowdhury et al. [20] has an uncertainty of ±1.2% (or about 5 m/s). This velocity uncertainty corresponds to a variation in stated Mach number of ±0.013 – 0.019 for the range of M_s of interest herein (typically for M_s between 1.1 and 1.6). This overall

uncertainty in M_s takes into account any slight variation across the test location (Fig. 1) and the uncertainty of the measurement system in detecting the arrival of the shock wave at each transducer port.

2.2 Dust-Layer Measurement Technique

A basic shadowgraph technique was employed for flow field visualization. The present experimental viewing area is approximately 76 mm wide by 50 mm high, with the image width being limited by the concave mirror diameter and the image height by the height of the window. The curved mirrors have a 76-mm diameter and 44-cm focal length, resulting in an F# of 5.8. A Photron Fastcam SA1.1 high-speed camera at a frame rate of 15,000 fps and 1-μs exposure is used in conjunction with a Mercury-Xenon, 70-W lamp to capture the fluid and dust layer interaction. This framing rate provides a 67-μs time difference between each image. The camera was set to an image area resolution of 768×624 pixels.

To understand dust entrainment into the post-shock gas flow, particle lifting is typically measured with respect to time or with respect to the shock-wave propagation. For each experiment, images are captured of the nitrogen and dust-layer interaction behind the incident shock wave. A typical image sequence of the dust-gas interaction behind a shock wave of M_s = of 1.32 is shown in Fig. 3. It can be observed that a normal shock wave is followed by the subsequent movement of the dust in the vertical, or y, direction. Note that the shadowgraph method provides a very good resolution of the

boundary between the edge of the bulk dust surface and the gas above it, particularly for the earlier portion of the experiment. Dust surface transition to instability occurs from image (c) to (d), as this behavior is indicative of all experimental runs but occurring at different times depending on the shock speed. As seen in the last frame of Fig. 3, the reflected shock wave arrives at the test section, and the data acquisition portion of the experiment is concluded.

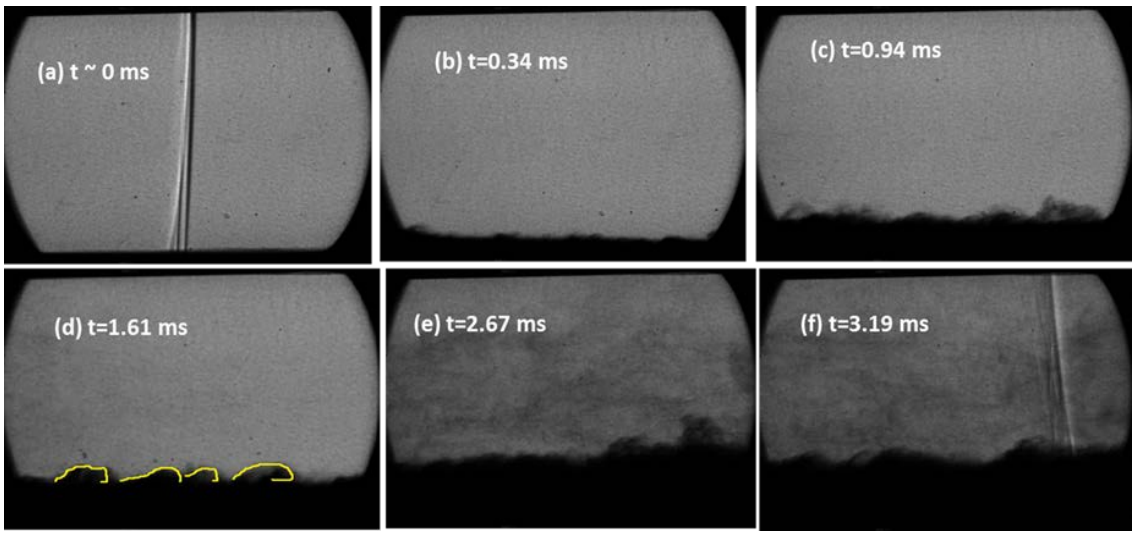

Figure 3 Images of limestone dust interaction in the flow behind a shock; M_s = 1.32. All captured images were for 15,000 frames per second with a 1-µs exposure time.

Dust height as a function of time is determined by examining the shadowgraph images. The corresponding shock wave propagation was derived from the shock velocity and time recorded by the camera using a known camera trigger location, which in the present tests is the pressure transducer upstream of the window, PT1 (see Fig. 1).

The initial and subsequent images taken during the experiments were analyzed frame-by-frame for spatially and temporally dependent dust measurements. Image analysis was performed by an in-house MATlab code designed to examine pixel-to-pixel variation and to identify the location of dust-gas boundaries and shock waves. A user-created MATlab add-on application, Image Measurement Utility [21], was used to calibrate the distance of each pixel in the image setup. Figure 4 presents a typical calibration image taken with a pair of digital calipers opened to 10.00 mm. A calibration line was drawn between the measuring edges of the calipers, and with a known 10.00 mm distance, a pixel calibration of 0.12 mm/pixel was established. Once this procedure establishes the image calibration, point-to-point calculations of post-shock dust height can be accurately made.

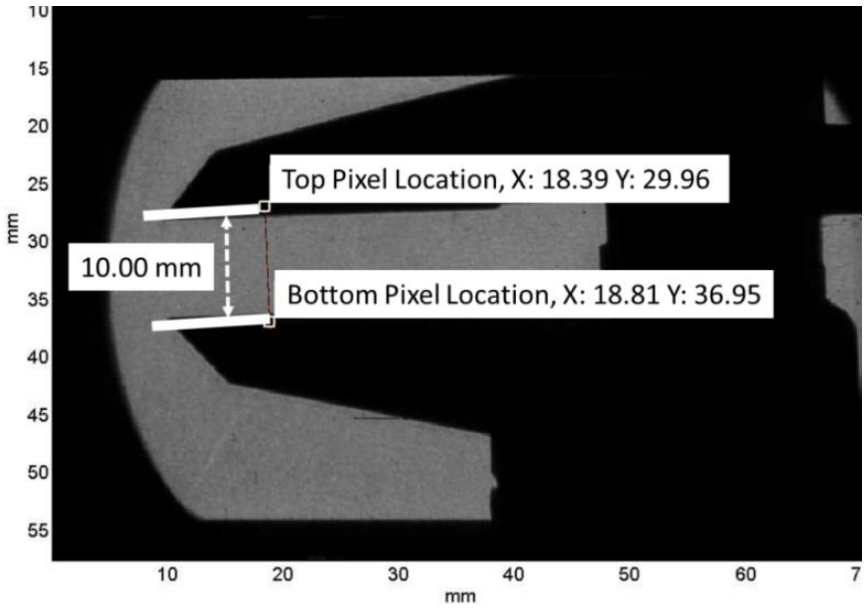

Figure 4 Image-Pixel calibration using calipers and the MATlab Image Measurement Utility.

To discern and measure a clear dust-gas boundary for recording dust-height variations, the images were converted from raw, indexed values to RGB. Pixel RGB values were examined to set thresholds correlating to shadowgraph density gradients. In Fig. 5, the incident-shock image is used to establish a fixed vertical reference plane at X = 460 to measure the fixed vertical height of the viewing window bottom and distance to the shock wave. Subsequent images continually measure dust heights from the vertical reference plane. The RGB image shown in Fig. 5 identifies the shock wave above a zero (0) threshold for green and blue pixel color values, as compared to the zero (0) green and blue values in the constant-density gas located in the space between the shock wave front at X = 134 and the vertical reference plane. The number of pixels at a constant height of Y = 368 are counted between the shock wave and vertical reference plane, and with the pixel calibration, shock wave distance is determined. The image frame rate, measured shock speed, and measured distance allow a precise time to be calculated to determine when the shock wave passes the vertical reference plane. As frames were 66.7 microseconds apart for a 15,000 fps rate (~3 ms total test time), the post-shock images were corrected by the elapsed time between the shock wave passing this plane and subsequent time-stamped images. For example, a $M_s = 1.32$ wave presents an elapsed time of 90.9 microseconds, which is a typical value.

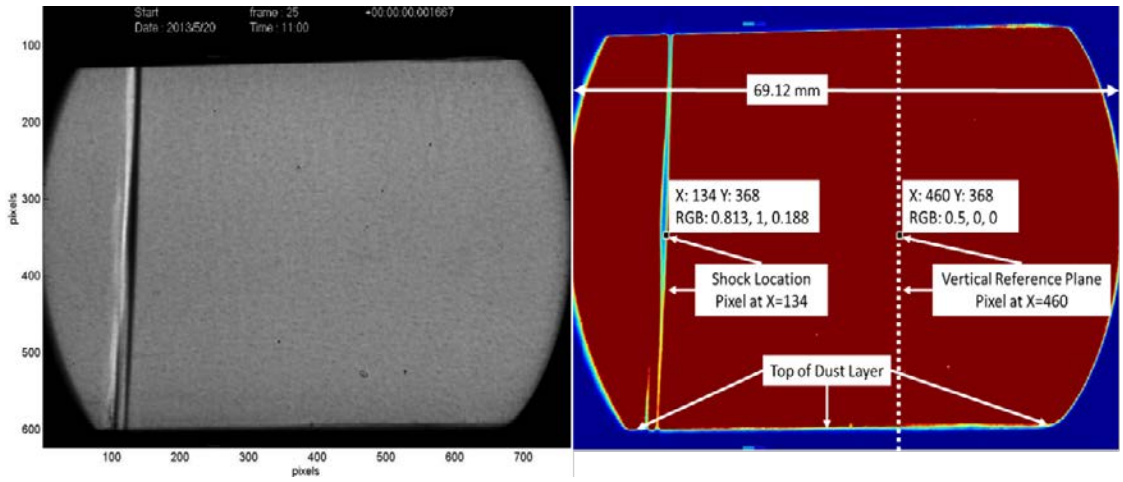

Figure 5 Incident Mach 1.32 shock wave raw indexed image (left) and RGB image (right) with RGB pixel values at vertical reference plane and shock wave.

The left image in Fig. 6 identifies a pre-shock horizontal reference plane at Y = 596, relative to which all subsequent dust-height measurements are referenced. This plane corresponds to the viewing window bottom and was identified to terminate in the gas at a zero (0) threshold blue pixel color value, as compared to the space between the image bottom and the horizontal reference plane. The right image in Fig. 6 is post-shock dust which is rising at the fixed vertical reference plane and above the horizontal reference plane, which is 1.45 mm above the top of the undisturbed dust layer. The zero (0) threshold blue pixel value is used on most of the subsequent images to identify the dust-gas boundary and to record dust-height measurements with time. Ultimately, the uncertainty in the determination of the dust-layer edge is within one pixel, since the RGB contrast goes to zero very dramatically at the dust-gas boundary. Therefore, the stated uncertainty for the dust height Y_d is ±0.12 mm; note that this is the precision to which the dust-gas interface can be determined from the image resolution. There is

additional uncertainty involved in defining the interface when there are time-dependent fluctuations in this interface as a result of the fluid mechanics of a given experiment. Hence, the overall uncertainty in the dust-gas interface is higher, particularly at later times, as shown later in this study.

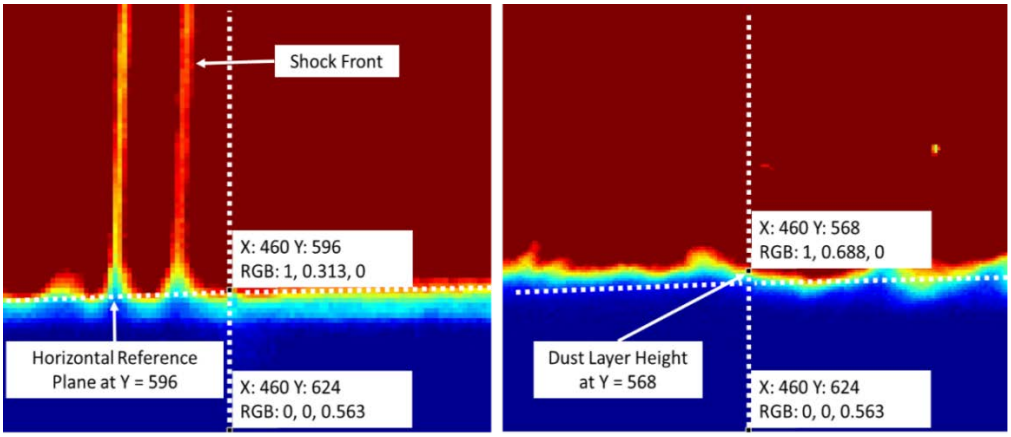

Figure 6 Pre-shock horizontal reference plane (left) and post-shock dust height measurement (right) with RGB pixel values at horizontal reference plane and dust-gas boundary.

In some cases at longer observation times, a background dust cloud can enter the observation area, increasing the uncertainty. This cloud is caused by residual dust deposits on the shock-tube walls from previous experiments being lifted and carried into the observation area. This uncommon event is addressed by slightly modifying threshold values to account for increased sensitivity in density variations. This adjustment provides an accurate representation of the boundary between areas that were filled with dust lifted from the initial dust layer, and those which are composed of background dust. Data are presented as the dust height rises with time at the vertical reference plane, with

height = 0 at the horizontal reference plane (window bottom), and time = 0 when the shock wave reaches the vertical reference plane.

2.3 Dust-Layer Setup

Experimental variables from test to test include initial pressure (P_1), shock Mach number (M_s), dust-layer thickness, and characteristics of the dust itself. A constant value of 67 kPa (500 torr) was used for P_1 herein, or initial test section pressure. For the test gas, nitrogen was used to render the atmosphere inert. After each experiment that employed dust, the inner surfaces of the shock tube were vacuumed and cleaned thoroughly with acetone. The dust-layer depth remained constant at 3.2 mm with the geometry shown in Fig. 1 throughout the experiments.

The coal-limestone mixtures were developed and tested in accordance with Table 1. The five (5) types of mixtures include all coal, all limestone, and a ratio by weight for the varied coal and limestone mixture content. Densities are listed and computed as the mixtures were weighed and placed into the 60.14 cm^3 dust tray shown in Fig. 1.

Table 1 Coal-limestone mixture test matrix with average mixture densities

Dust Sample(s)	Dust Parameters			Test Cases		
	Weight Mixture Ratio (Coal:Limestone)	Average Mixture Mass (g)	Average Mixture Density (g/cm3)	Mach 1.24	Mach 1.57	Total Sample Tests
100% Coal	1:0	24.8	0.413	2	2	4
75% Coal / 25% Limestone	3:1	19.8	0.329	2	2	4
50% Coal / 50% Limestone	1:1	15.2	0.253	2	2	4
25% Coal / 75% Limestone	1:3	11.8	0.197	2	2	4
100% Limestone	0:1	11.1	0.188	1	1	2
Accumulated Averages =>		16.7	0.278	Total Tests = 18		

The limestone mixed into the coal in Table 1 was undried and stored at standard temperature and pressure (STP) conditions. As the limestone moisture content is reduced, dust dispersion is expected to change. Table 2 shows the test cases for the dried limestone samples at the respective Mach numbers shown. Undried limestone samples were tested at the same Mach numbers for comparison. Positive numbers indicate the moisture content was removed from the samples prior to the experiments. All samples were dried at elevated temperatures for approximately 192 hours. The weight data for the dried samples are recorded in Table 2, and moisture content for the dried samples was calculated in accordance with Equation 1.

$$Percent\ Moisture\ Content = \frac{Wet\ Weight - Dry\ Weight}{Wet\ Weight} \times 100 \qquad \text{(Equation 1)}$$

Table 2 Dried limestone test cases with percent moisture content

Mach Number	Dust Parameters	
	Sample Weight (g)	Moisture Content
1.1	17.01	0.52%
1.23	19.85	1.02%
1.4	24.81	1.00%

All limestone used in the test cases from Tables 1 and 2 used the same size, batch, and type of limestone acquired from the same vendor. All undried limestone was stored at standard temperature and pressure (STP) conditions. The coal-limestone mixtures and limestone-only samples were evenly spread and leveled with the top of the dust-tray, which is coincident with shock tube's bottom surface. This positioned the dust to be recessed below the incident shock wave. Once the shock wave entered the test section, the dust was dispersed and measurements were made.

Figure 7 shows the dust trays loaded with the appropriate mixtures from Table 1. The 100% limestone image is undried. As the coal content is reduced, and the limestone content increased, the dust tends to maintain a more limestone-only-like texture with a grey, uniform color exhibiting a well-mixed sample.

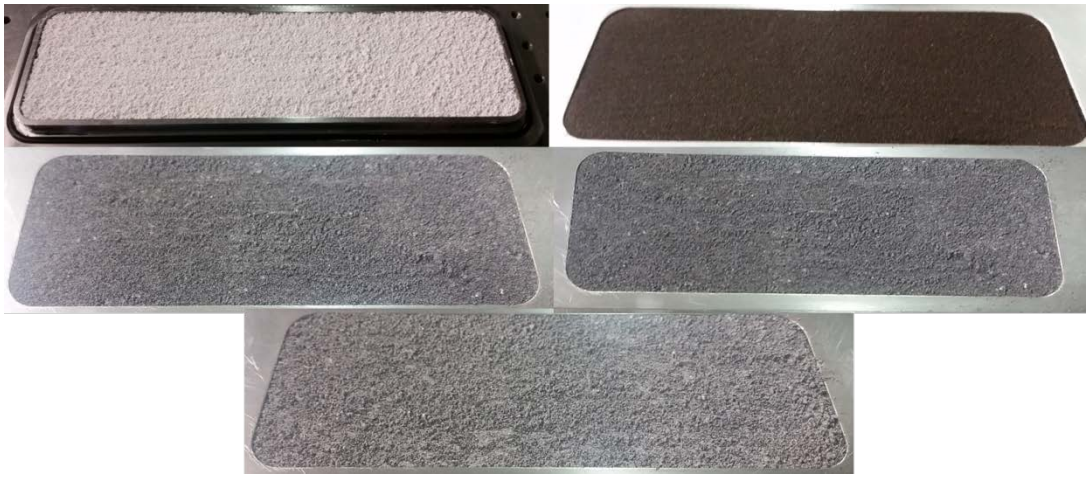

Figure 7 Images of coal-limestone mixtures in the dust-tray for test cases from Table 1. In a clockwise direction, starting at the top left, 100% limestone, 100% coal, 50% coal, 25% coal, and 75% coal representative samples.

Once the dust tray was loaded for each experiment, the tray was placed into the bottom of the shock tube and sealed into the bottom section of the shock tube as shown in Section 3.1. All data are then captured and processed as detailed in Section 3.2. As the experimental setup is concluded, the focus now shifts to material characterization and the experimental results in the following chapter.

3. MATERIAL CHARACTERIZATION

For the present study, dust layers were limestone dust obtained off-the-shelf, and the coal was Wyoming bituminous. For the limestone, the SEM images in Fig. 8 and a Beckman coulter counter assessment suggested an average particle size of 4.2 microns. Figure 8 displays SEM images of the limestone dust particles in the coal-limestone mixtures and undried samples used in the experiments described herein. Images show a spore-like shape.

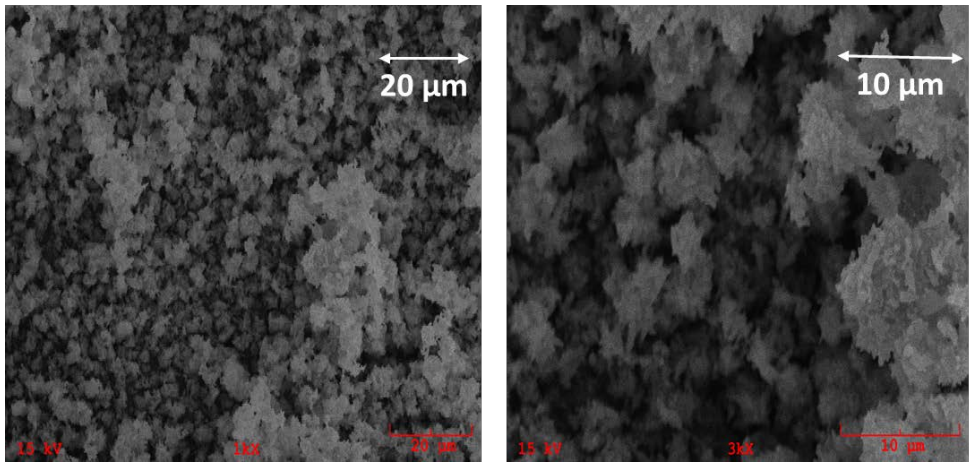

Figure 8 SEM images of 100% undried limestone powder utilized herein, at two different magnifications. Average particle sizes closer to the measured value of 4.2 microns are evident in the image, with some agglomerations of approximately 20-30 microns, which may affect dust lifting height in contrast to a loose, unadhered, 4.2-micron sample.

The coal was pulverized and sieved to a target maximum size of 150 μm. Figure 9 shows an SEM for a 100% coal sample with particles ranging from roughly 50-200 μm. The coal surface appears to be rough with uneven surfaces.

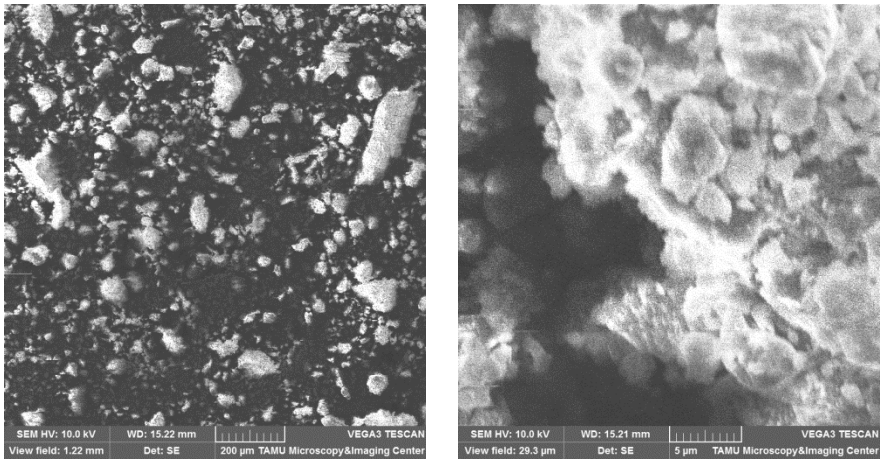

Figure 9 SEM images of 100% Coal. Coal particles range from 50-200 μm (left image) with rough and uneven surfaces (right image).

Figure 10 shows the coal-limestone mixture of 25% coal. Networks of particles are forming, with limestone particles agglomerating to coal particles.

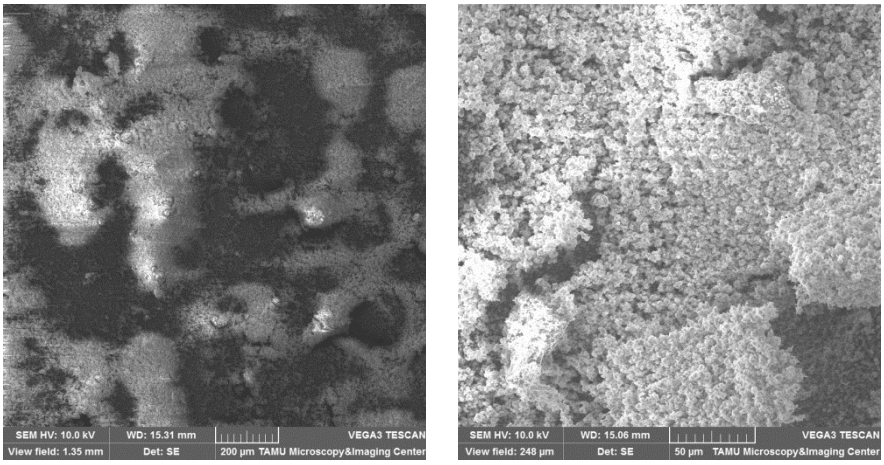

Figure 10 SEM coal-limestone mixture images of 25% coal / 75% limestone. Limestone appears to adhere to coal particles (right image) with clusters of 500 µm and networks forming (left image).

Figure 11 shows the coal-limestone mixture of 50% coal. Limestone is covering coal particles, and networks of particles are larger than 800 µm.

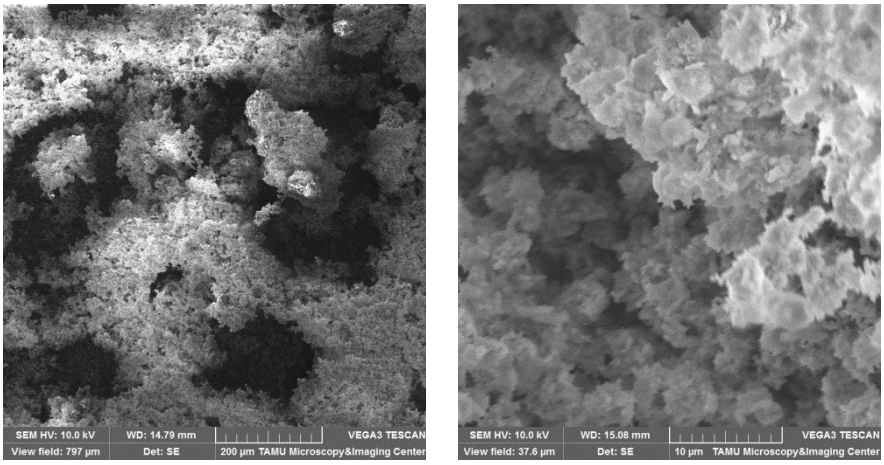

Figure 11 SEM coal-limestone mixture images of 50% coal / 50% limestone. Limestone appears to adhere to coal particles (right image) with clusters of 200 µm and networks larger than 800 µm (left image).

Figure 12 shows the coal-limestone mixture of 75% coal. Limestone is covering coal particles, with clusters of 400 μm and networks of particles are larger than 500 μm.

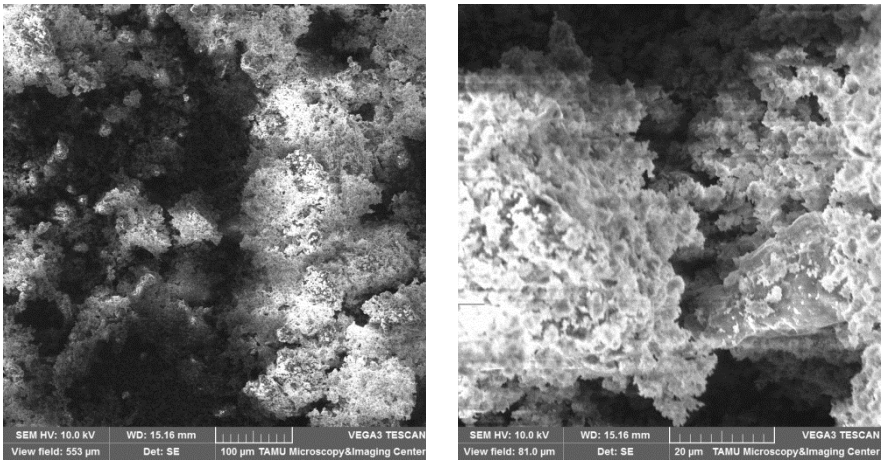

Figure 12 SEM coal-limestone mixture images of 75% coal / 25% limestone. Limestone appears to adhere to coal particles (right image) with clusters of 400 μm and networks larger than 500 μm (left image).

Based on the SEM images, the overall trend is that the limestone (undried state) adheres to the coal, causing agglomerations. These agglomerations are good for the likelihood of the coal having less surface area available for ignition in the events discussed in Chapter 1. The lifting force is also expected to be affected by the agglomerations, and the following results section shows the relative dust lifting heights between the different coal-limestone mixtures and the effect of moisture reduction on the limestone.

4. EXPERIMENTAL RESULTS

The experimental results were intended to quantify the dust dispersion from the different coal-limestone mixtures, and coupled with the dried limestone only dispersion, should help in understanding what factors affect dust growth rates and overall dispersion heights. The first result is for the coal-limestone mixtures (see Fig. 13 and 15 later), which correspond to the Table 1 test matrix. The second result is the dried and undried limestone comparison (see Fig. 17), in which the dried samples moisture content corresponds to Table 2. These two results illustrate the overall dust dispersion behind a moving shock wave, as the wave passes, and the dust is lifted into the atmosphere over a final time ranging from about 2.8 - 3.2 ms per test. Linear dust growth regions, which exhibit laminar behavior, were fit to an R-squared value of 0.95 or better.

4.1 Coal-Limestone Mixture Results

The Mach 1.24 coal-limestone mixture results in Fig. 13 show an increasing trend in the linear portions of the growth rates ($\frac{\mathbf{dY_d}}{\mathbf{dt}}$) of the dust height prior to 2.5 ms, as limestone content is increased in the mixtures. The 75% coal mixture has over a 40% increase in growth rate as compared to the 100% coal. Overall dust heights show an increasing trend with an increase in the limestone content. Table 3 has the linear growth rates for each sample. The delay time when dust growth is first observed after the passing normal shock wave, and the transition time at which the linear growth portion

turns to a fluctuating, unsteady behavior and the time span between the two are included in Table 3 (linear time span).

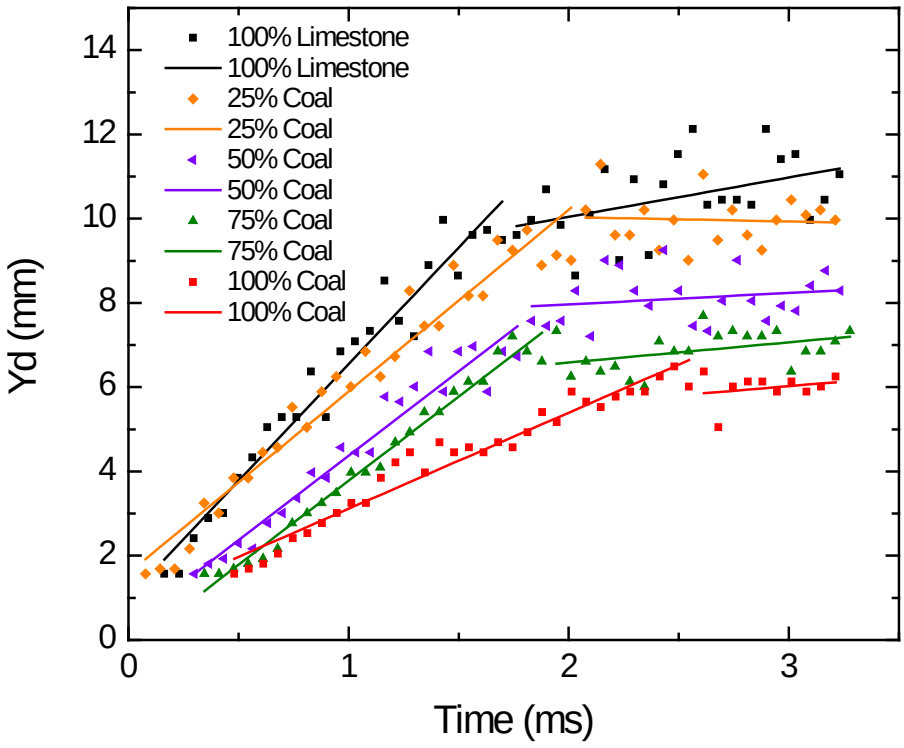

Figure 13 Coal-limestone mixture results at $M_s = 1.24$. Solid lines show overall trend of each mixture from Table 1.

As noted in Table 3, the linear growth rates increase as the limestone content increases from 100% coal to 100% limestone. As the growth rates increase, linear time spans decrease and the tendency for the dust to transition to unsteady behavior begins earlier as limestone content increases in the mixtures, except in the 25% coal mixture

where the span and transition times are larger and later than the lower content limestone samples. The 25% coal sample has the lowest delay time. Following the same trend, the delay and transition times reduce with an increase in limestone content. The unsteady period after the transition time, for each sample, increased in average overall dust height with increased limestone content as Fig. 13 exhibits.

Table 3 Coal-limestone linear growth region characteristics for $M_s = 1.24$

Dust Sample(s)	Linear Growth Rate dY/dt (mm/ms)	Linear Time Span (ms)	Delay Time (ms)	Transition Time (ms)
100% Coal	**2.25**	**2.13**	**0.48**	**2.61**
75% Coal / 25% Limestone	**3.96**	**1.60**	**0.34**	**1.94**
50% Coal / 50% Limestone	**3.98**	**1.53**	**0.30**	**1.83**
25% Coal / 75% Limestone	**4.33**	**2.07**	**0.08**	**2.14**
100% Limestone	**5.38**	**1.60**	**0.16**	**1.76**

Figure 14 shows a shadowgraph of the dust behavior just after the transition time periods noted in Table 3. As the limestone content is increased, dust grows faster, larger, and tend to transition into larger instabilities on the dust-gas boundaries. In comparing to the Fig. 14 dust dispersion, the 100% coal sample exhibits small particles above the dust boundary, as compared to the samples with limestone which tend to bind the mixture together.

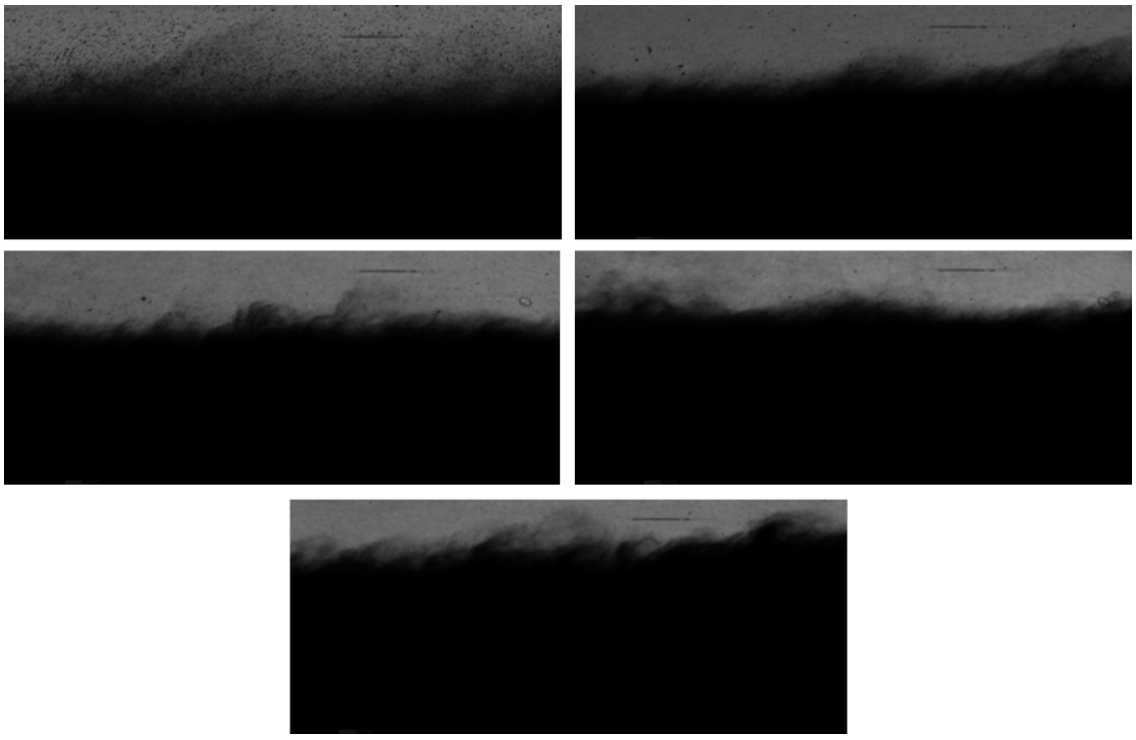

Figure 14 Coal-limestone unsteady post-transition time shadowgraphs for M_s = 1.24. From left to right, top to bottom: 100% coal, 75% coal, 50% coal, 25% coal, and 100% limestone.

The Mach 1.57 coal-limestone mixtures in Fig. 15 show an increasing trend in the linear portions of the growth rates ($\frac{dY_d}{dt}$) of the dust growth regime prior to 0.85 ms, as limestone content is increased in the mixture. The 75% coal mixture has nearly a 40% increase in growth rate as compared to the 100% coal. Further increase in limestone content has a small effect on growth rate. Overall dust heights show an increasing trend as limestone content increases, except the 25% coal sample which is nearly even with the 50% coal data. The 100% limestone samples exhibit similar growth rates as the 25%

and 50% coal samples, and then disperse high above all other samples in the unsteady region. Table 4 has the linear growth rates for each sample. The delay time when dust growth is first observed after the passing normal shock wave, transition time at which the linear growth portion turns to a fluctuating unsteady behavior and the time span between the two are included in Table 4 (linear time span).

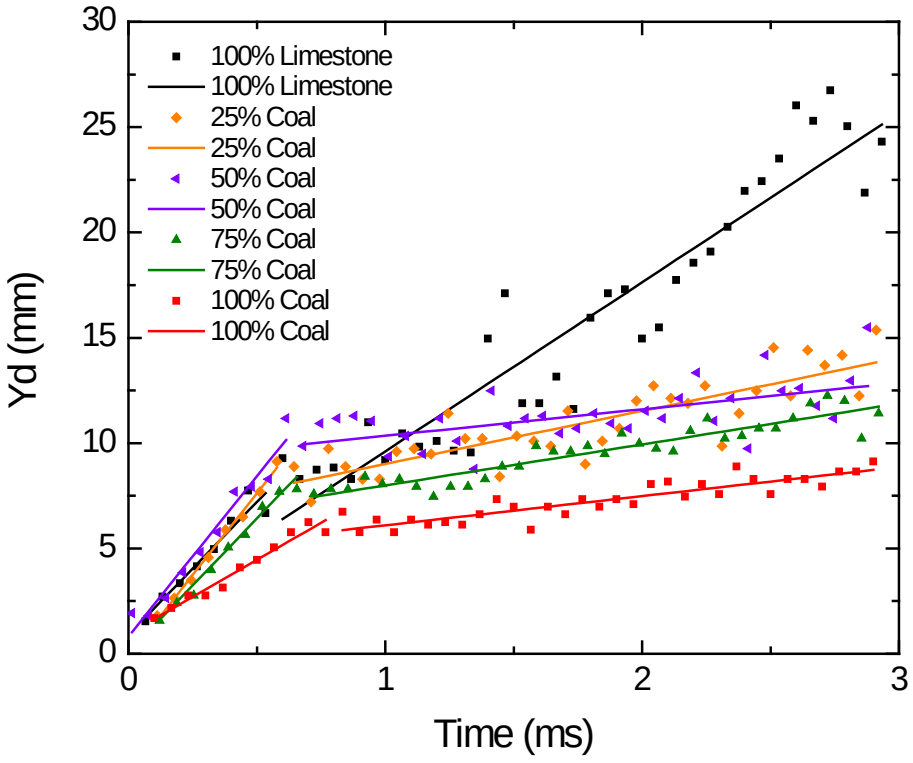

Figure 15 Coal-limestone mixture results at M_s = 1.57. Solid lines show overall trend of each mixture from Table 1.

As noted in Table 4, the linear growth rates increase as limestone content increases from 100% coal to 100% limestone, except at 100% limestone where it is slightly lower than the trend. As the growth rates increase, linear time spans decrease and the tendency for the dust to transition to unsteady behavior begins earlier as limestone content increases in the mixtures, except in the 50% coal mixture which has span and delay times that are larger and earlier than the trend. The 50% coal sample has the lowest delay time, with the other samples at nearly constant values. The transition times reduce with an increase in limestone content. The unsteady period after the transition time, for each sample, increased in average overall dust height with increased limestone content as Fig. 15 exhibits.

Table 4 Coal-limestone linear growth region characteristics for $M_s = 1.57$

Dust Sample(s)	Linear Growth Rate dY/dt (mm/ms)	Linear Time Span (ms)	Delay Time (ms)	Transition Time (ms)
100% Coal	**6.99**	**0.73**	**0.10**	**0.83**
75% Coal / 25% Limestone	**11.46**	**0.60**	**0.12**	**0.72**
50% Coal / 50% Limestone	**14.32**	**0.67**	**0.01**	**0.68**
25% Coal / 75% Limestone	**14.52**	**0.53**	**0.11**	**0.64**
100% Limestone	**13.46**	**0.53**	**0.07**	**0.60**

Figure 16 shows a shadowgraph of the dust behavior just after the transition time periods noted in Table 4. As the limestone content is increased, dust grows faster, larger, and transition more quickly into larger instabilities on the dust-gas boundaries. In comparing Fig. 16 dust dispersion, the 100% coal sample exhibits small particles above the dust boundary, as compared to the samples with limestone which tend to bind the mixture together. This is the same result as the Mach 1.24 coal-limestone mixture test cases.

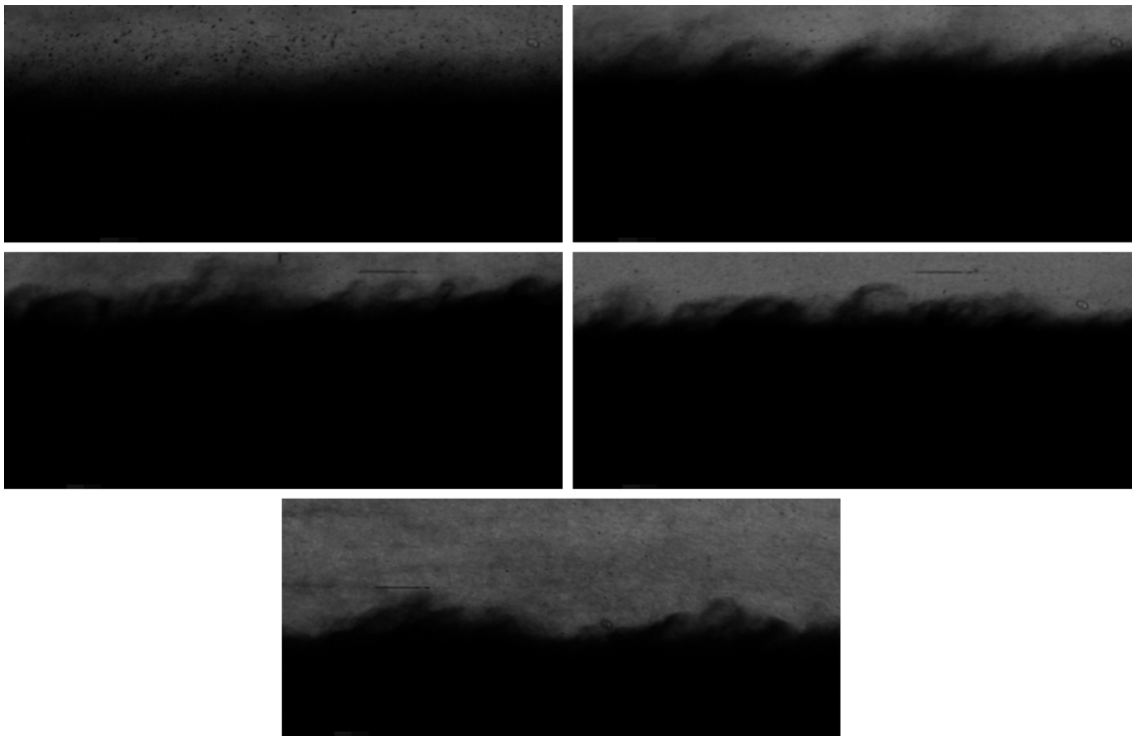

Figure 16 Coal-limestone unsteady post-transition time shadowgraphs for $M_s = 1.57$. From left to right, top to bottom: 100% coal, 75% coal, 50% coal, 25% coal, and 100% limestone.

4.2 Dried and Undried Limestone Results

As the limestone content was shown to have an effect on the coal-limestone mixtures, the limestone was further investigated. This experimental campaign was based on reducing the moisture content of the limestone, by oven drying, to see the effects on dust growth. Table 2 represents the moisture content in the three (3) targeted Ms = 1.1, 1.23, and 1.4. Corresponding to the Table 2 samples, Fig. 17 shows the time-evolved data from the limestone-only tests, which include undried samples tested at the same M_s as the dried.

These results represent the differing of dust dispersion heights due to the dried and undried limestone samples and shock Mach number. Based on the three Mach numbers, namely 1.1, 1.23, and 1.4, the trending data show an increase in lifting height for the dried samples, as compared to the undried samples. Dried sample dust heights varied from -30 to +32, -15 to +44, and -36 to +45 percent differences from undried samples for Ms = 1.1, 1.23, and 1.4, respectively. The majority of the data points are greater values for the dried samples. The solid lines in Fig. 17 represent initial linear growth rates, or $\frac{d(Y_d)}{dt}$, where the dust-gas boundary remains laminar. The growth rates are larger for the dried samples, as compared to the undried samples.

When the dust height is plotted as a function of time, the initial trend appears to be linear, as seen in Fig. 17. However, at some later time (about 2 ms for M_s = 1.23) the rate of growth slows down considerably. In this second regime, note also that the data

representing the dust height have much larger scatter, due primarily to the surface structures that begin to appear.

Figure 17 also illustrates the transition from the higher growth rate to the lower one appearing to be dependent on the shock Mach number, where the higher M_s leads to a transition point at earlier times when compared to the lower M_s cases. These results are typical of the experiments performed to date in the facility [20]. The transition points appear to increase for the dried samples at M_s = 1.1 and 1.23, with M_s = 1.4 following the opposite trend, as compared to the undried samples at a constant Mach number.

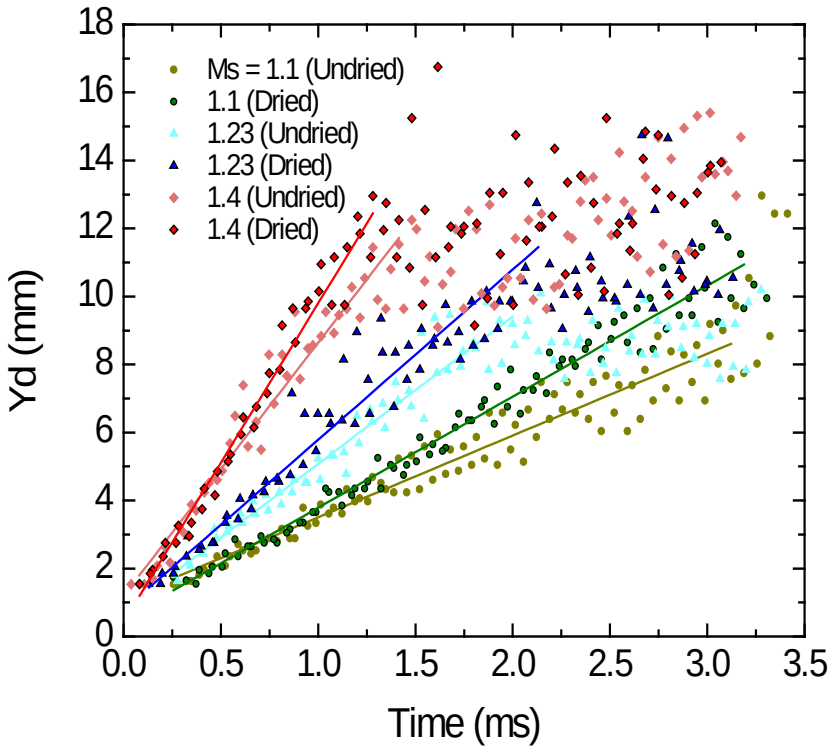

Figure 17 Dried and undried limestone sample comparison for measured dust height, Yd, as a function of time for three different Ms (1.1, 1.23, and 1.4). Dried sample linear growth regimes (solid lines) increase in the laminar regions, as compared to the undried samples at the corresponding Mach numbers.

As noted in Table 5, the linear growth rates are larger for the dried samples, as compared to the undried samples at constant Mach numbers. Both undried and dried sample categories exhibited increased growth rates as Mach numbers increased. Delay times were greater for dried samples at Mach 1.1 and 1.4, with the opposite trend at Mach 1.23. Transition times were difficult to extract from data, as the exact moment of the laminar transition may vary. Nonetheless, whether the samples are dried or undried, the data show a decrease in transition times as the shock Mach numbers are increased. Also, the dried limestone transitioned later, as compared to the undried samples, except the dried sample at Mach 1.4 where the transition time was the lowest of all the samples.

Table 5 Dried and undried correlated values presented in Fig. 18 to predict dust growth rates with known shock Mach numbers ranging from 1.1 to 1.4. Time values indicate dust delay rise times after passing normal shock and transition times from laminar to unstable regimes.

Undried Limestone				**Dried Limestone**			
Correlation		**Critical Times**		**Correlation**		**Critical Times**	
Mach	$d(Y_d)/dt$ (mm/ms)	Delay Times (ms)	Transition Times (ms)	Mach	$d(Y_d)/dt$ (mm/ms)	Delay Times (ms)	Transition Times (ms)
1.1	2.40	0.27	3.13	1.1	3.27	0.31	3.25
1.23	4.33	0.27	2.01	1.23	5	0.16	2.16
1.4	7.44	0.06	1.39	1.4	9.37	0.11	1.31
D(Yd)/Dt	**16.87**			**D(Yd)/Dt**	**20.63**		
Intercept	**-16.24**			**Intercept**	**-19.76**		

In Fig. 18, correlations are shown for the linear growth regions for a given shock Mach number, M_s. Linear growth rates varied from 3.27 to 2.4, 5 to 4.3, and 9.4 to 7.4

mm/ms for M_s = 1.1, 1.23, and 1.4, respectively; where the larger values at specific Mach numbers were the dried samples. Clearly, the dried samples are rising faster and maintaining larger overall dust height values at the corresponding Mach numbers.

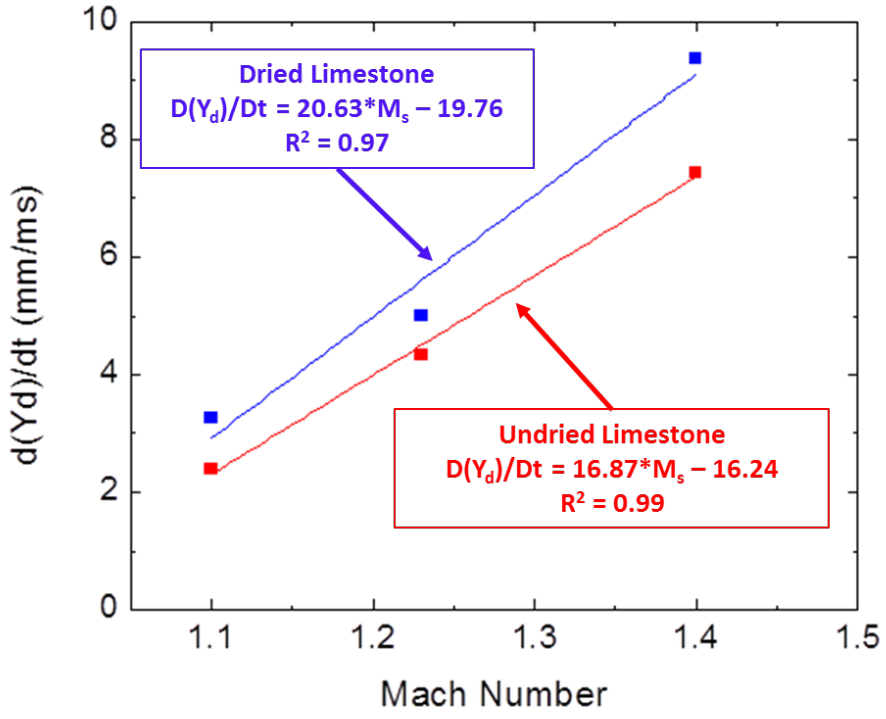

Figure 18 Dried and undried limestone sample comparison for laminar correlated linear growth rates, $\frac{D(Y_d)}{Dt}$, as a function of Mach number, M_s (1.1, 1.23 and 1.4). Dried sample correlations result in larger growth rates, as compared to undried samples at a selected Mach number range from 1.1 to 1.4.

Based on three shock Mach numbers, namely M_s = 1.1, 1.23, and 1.4, the trending data show an average increase of 10% in overall lifting heights and 20% in initial linear growth rates for the moisture-reduced, dried samples, as compared to undried samples stored in standard temperature and pressure (STP) conditions.

5. CONCLUSION

Dust growth behavior studied in the shock tube discussed led to many important results toward a better understanding of what factors affect coal dust dispersion in areas where secondary explosion hazards exist. The variation of M_s from 1.1 to 1.57 was selected to capture the various conditions a blast wave may produce in coal mines or industrial settings during a primary explosion. In industrial settings, limestone is introduced in intimate contact with surrounding loose coal particles and used as a mechanism to mitigate the ignition of coal particles lifted and heated from a passing shock wave. The limestone is expected to render the coal inert. Results presented in the previous chapter attempt to simulate these energetic conditions by matching the shock wave speeds (not temperature and pressure), while varying coal-limestone mixture ratios and studying the effect that limestone moisture content has on dust dispersion.

The coal-limestone mixtures and limestone moisture presented in Tables 1 and 2, with test results in Figures 13, 15, and 17 are summarized in Table 6 for select parameters affecting dust dispersion. Overall dust dispersion heights increase with increasing Mach number for all samples tested. Table 6 targets time parameters that effect how quickly the dust transitions to an unstable boundary layer, readily increasing the chances of ignition through increased mixing and dispersion. Transient high temperatures behind a shock wave can quickly appear and vanish, removing the necessary ignition temperature for the particles to react. Ignition mitigation criteria would be reducing dispersion and increasing time at which transition occurs.

The highest growth rate, shortest transition time, and largest average dust height will increase the ability of the dust sample to be better mixed with the gas above it. Highlighted values which pose the most danger for ignition are shown in Table 6. Increasing limestone content while maintaining the lowest possible dust dispersion would both help the mixture remain inert and expose less coal particle surface area to the reactive atmosphere.

With these issues in mind, the most unfavorable conditions are a coal-limestone mixture of 75% coal and dried limestone. The most favorable conditions are a coal-limestone mixture of 25% coal and undried limestone; however, note that the transition times for undried limestone are less than the dried ones creating a possible unfavorable condition. These parameters were chosen with no consideration of the likelihood of the mixture to react, instead, they were chosen in respect to the fluid-particle dispersion dynamics. A reactive study would be necessary, and therefore recommended, for a complete understanding of the fluid-particle and chemical interactions. In addition, limestone may bond or agglomerate more readily to coal particles when undried, reducing the likelihood of ignition.

Table 6 Critical time parameters for time-sensitive dust dispersion

Sample	Linear Growth Rates d(Yd)/dt (mm/ms)			Transition Time (ms)			Average Dust Height (mm)		
Limestone Mixture Percentage (by weight)	M_S = 1.24	M_S = 1.57	% Change	M_S = 1.24	M_S = 1.57	% Change	M_S = 1.24	M_S = 1.57	% Change
0	2.25	6.99	68%	2.61	0.83	-213%	4.69	6.45	27%
25	3.96	11.46	65%	1.94	0.72	-169%	5.46	8.60	36%
50	3.98	14.32	72%	1.83	0.68	-170%	6.27	10.02	37%
75	4.33	14.52	70%	2.14	0.64	-232%	7.54	9.90	24%
100	5.38	13.46	60%	1.76	0.60	-194%	8.29	13.75	40%
Limestone Only Samples	M_S = 1.1	M_S = 1.23	M_S = 1.4	M_S = 1.1	M_S = 1.23	M_S = 1.4	M_S = 1.1	M_S = 1.23	M_S = 1.4
Undried Limestone	2.40	4.33	7.44	3.13	2.01	1.39	5.58	6.92	9.64
Dried Limestone	3.27	5.00	9.37	3.25	2.16	1.31	6.34	7.88	10.12

In conclusion, the coal-limestone mixtures were combined to have homogenous mixtures, as field conditions may have a top-layer of limestone above the coal. This would affect the dynamics conceived above. Also, it is convenient that undried limestone is more favorable than dried; however, in dry or hot environments this unfavorable condition may present itself. Conceivably, the effective moisture reduction in the samples led to fewer agglomerations and/or reduced sample densities, influencing the ability of lift forces to act on the particles. The moisture-reduced effect increases dust dispersion and growth rates. As the dried limestone increased dust dispersion, this is effectively increasing the likelihood of promoting secondary explosion hazards. Since reduction of secondary explosion hazards is important, future studies and safety

precautions should focus on reactive chemistry and understanding the mitigation techniques for the specific environment, respectively.

REFERENCES

1. Eckhoff, R. K.: Current Status and Expected Future Trends in Dust Explosion Research, Journal of Loss Prevention in the Process Industries **18**, pp. 225-237 (2005).

2. Houim, R., Oran, E.: Numerical simulation of dilute and dense layered coal-dust explosions, Proceedings of the Combustion Institute **35**, 2083-2090 (2015).

3. Kanno, T., Matsuo, A.: Numerical Investigation of Dust Lifting behind a Shock Wave using LPI Method, Tenth International Symposium on Hazards, Prevention, and Mitigation of Industrial Explosions (X ISHPMIE), Bergen, Norway, 10-14 June (2014).

4. Gerrard, J. H.: An experimental investigation of the initial stages of the dispersion of dust by shock waves, Brit. J. Appl. Phys. **14**, 186-192 (1963).

5. Fletcher, B.: The interaction of a shock with a dust deposit, J. Phys. D: Appl. Phys. **9**, 197-202 (1976).

6. Merzkirch, W., Bracht, K.: The erosion of dust by a shock wave in air: Initial stages with laminar flow, Int. J. Multiphase Flow **4**, 89-95 (1978).

7. Hwang, C. C.: Interaction of a coal dust-bed with shock-induced air stream, W. Merzkirch (ed.), Flow Visualization II, 547-551 (1982).

8. Tateuki, S., Takashi, A.: The effects of particle size on shock wave dust deposit interaction, Proc. of the 14th Intern. Symp. Space Technol. and Sci., 483-490 (1984).

9. Boiko, V. M. and Papyrin, A. N.: Dynamics of the formation of a gas suspension behind a shock wave sliding over the surface of a loose material, Combust. Expl. Shock Waves **23**, 231-235 (1987).

10. Fedorov, A. V.: Mixing in Wave Processes Propagating in Gas Mixtures (Review), Combustion, Explosions and Shock Waves **40**, 17-31 (2004).

11. Klemens, R., Zydak, P., Kaluzny, M., Litwin, D., Wolanski, P.: Dynamics of dust dispersion from the layer behind the propagating shock wave., J. Loss Prev. Process Ind. **19**, 200-209 (2006).

12. Fedorov, A. V., Fedorchenko, I. A.: Computation of Dust Lifting behind a Shock Wave Sliding along the Layer Verification of the Model, Combust., Expl., Shock Waves **41**, 336-345 (2005).

13. Fedorov, A.V., Fedorova, N.N.: Numerical simulations of dust lifting under the action of shock wave propagation along the near-wall layer, J. Phys. IV (France) **12**, Pr. 7-97-Pr. 7-104 (2002).

14. Khmel, T.A., Fedorov, A.V.: Interaction of a shock wave with a cloud of aluminum particles in a channel, Combust. Expl. Shock Waves **38**, 206-214 (2002).

15. Sakakita, H., Hayashi, A. K., Ivandaev A. I.: Numerical simulation of shock wave interaction with powder layers, K. Takayama (ed.), Shock Waves, Springer, Heidelberg (1992).

16. Klemens, R., Wolański, P., Kosiński, P., Korobeinikov, V.P., Semenov, I.V., Markov, V.V., Menshov, I.S.: On combustion and detonation behind a shock wave propagating over dust layer, Khim. Fiz. **20**, 112-118 (2001).

17. Skjold, T., Eckhoff, R.K., Arntzen, B.J., Lebecki, K., Dyduch, Z., Klemens, R., Zydak, P.: Simplified modeling of explosion propagation by dust explosion in coal mines, 5th International Seminar on Fire and Explosion Hazards, Edinburgh, UK, 302-313 (2007).

18. Ilea, C., Kosinski, P., Hoffmann, A.C.: The effect of polydispersity on dust lifting behind shock waves, Powder Technology **196**, 194-201 (2009).

19. Hwang, C.C.: Initial stages of the interaction of a shock wave with a dust deposit, Int. J. Multiphase Flow **12(4)**, 655-666 (1986).

20. Chowdhury, A.Y, Marks, B.D, Johnston, H.G, Mannon, M.S, Petersen, E.L: A new facility for studying shock-wave passage over dust layers, Shock Waves - An International Journal on Shock Waves, Detonations and Explosions, SHOC-D-14-00095R3 (2015).

21. Neggers, J.: Image Measurement Utility. MATLAB Central. N.p., (2012). Web.